Supporting Information

Gold-Nickel Phosphide Heterostructures for Efficient Photocatalytic Hydrogen Peroxide Production from Real Seawater

Wei Wang,[a,b] Qiang Luo,*[b] Jinyang Li,[b] Yunhong Li,[b] Linqian Li,[b] Xiaobing Huo,[b] Xiwen Du,[a] Ning Wang*[b]

[a]*Institute of New Energy Materials, School of Materials Science and Engineering, Tianjin University, Tianjin, 300072, P. R. China*

[b]*State Key Laboratory of Marine Resource Utilization in South China Sea, Hainan University, Haikou, 570228, P. R. China*

*Corresponding author

E-mail: luo-q11@foxmail.com

wangn02@foxmail.com

The calculation of HOMO and LUMO levels.

The HOMO and LUMO are calculated as follows:

$$E_{HOMO} = -\left(E_{onset}^{ox} - E_{ferrocene} + 4.8\right) eV$$

$$E_{LUMO} = -\left(E_{onset}^{red} - E_{ferrocene} + 4.8\right) eV$$

Where E_{onset}^{red}, E_{onset}^{ox} and $E_{ferrocene}$ are the reduction potential, onset of oxidation and the oxidation potential of ferrocene, respectively [1,2].

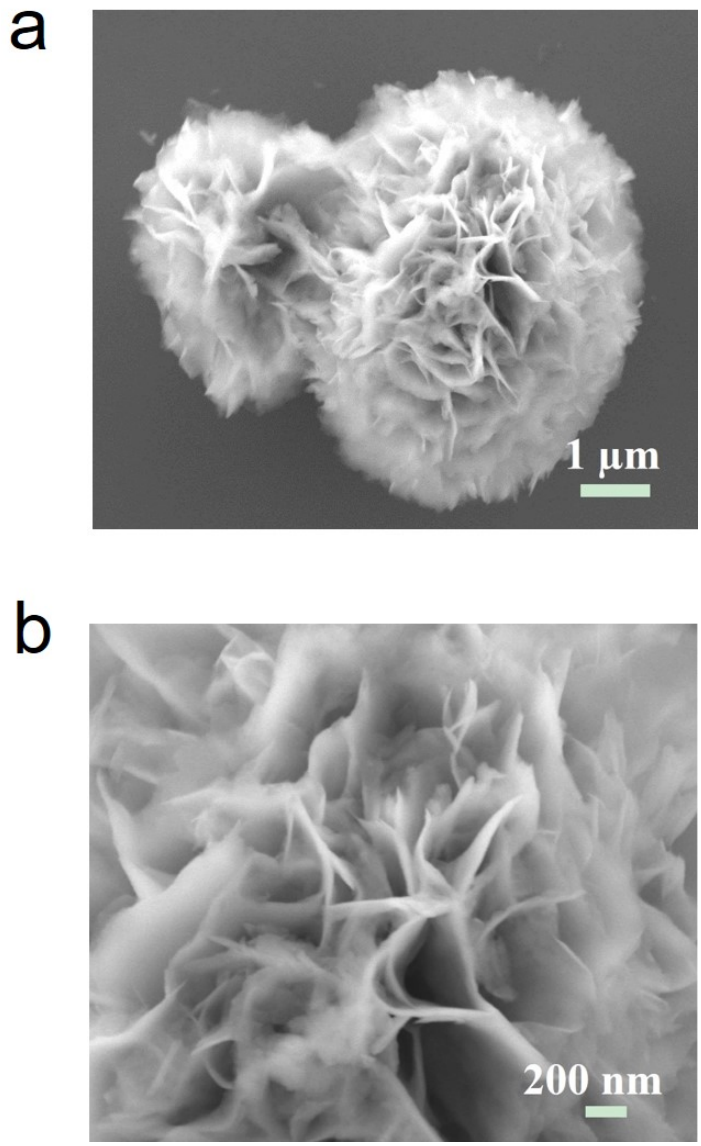

Fig. S1 SEM images of $Ni(OH)_2$ precursor.

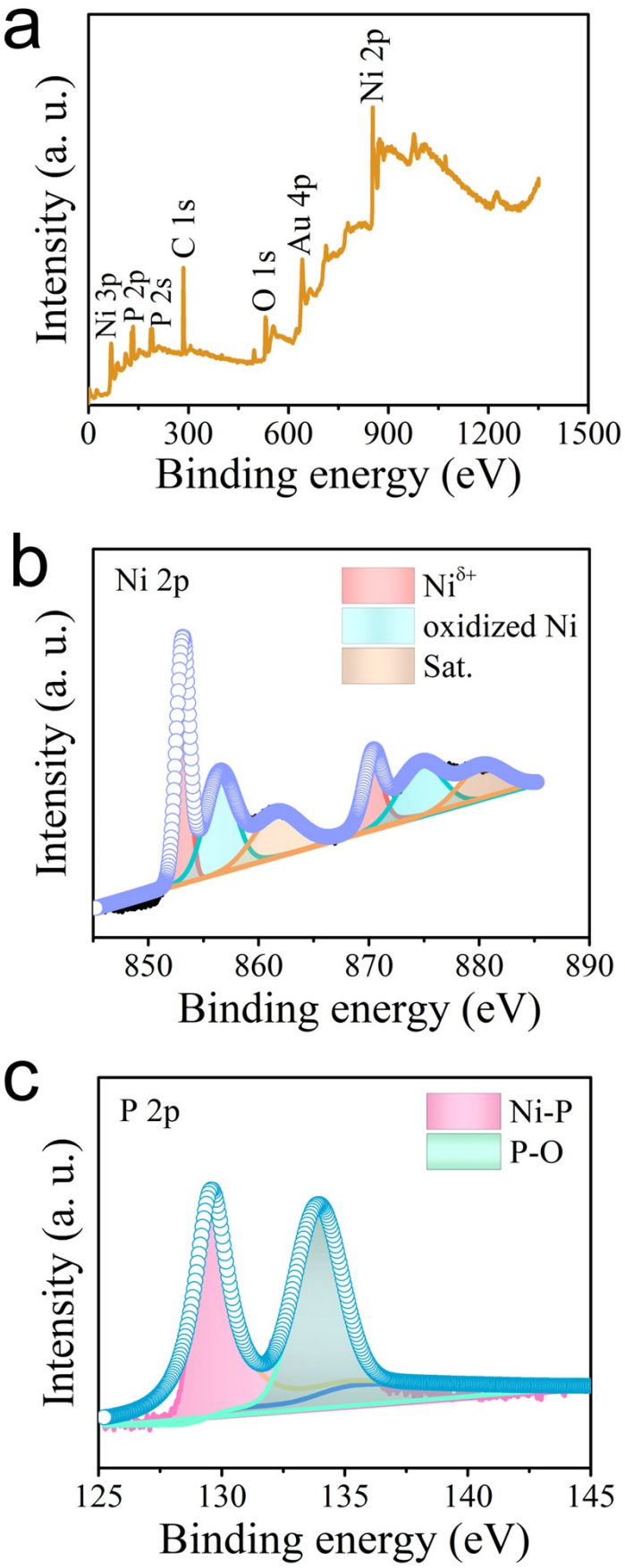

Fig. S2 XPS spectra of Au@Ni_5P_4. (a) survey, (b) Ni 2p and (c) P 2p, respectively.

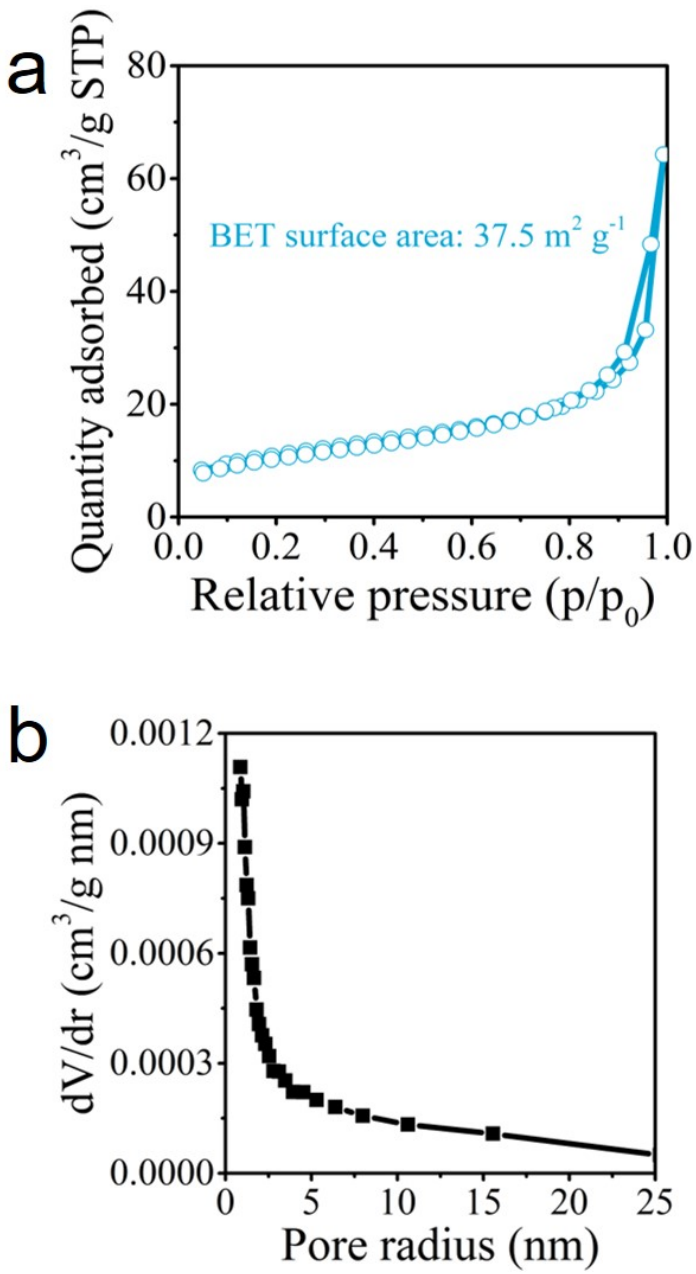

Fig. S3 (a) Nitrogen adsorption-desorption isotherms of Ni_5P_4, and (b) The corresponding pore size distribution.

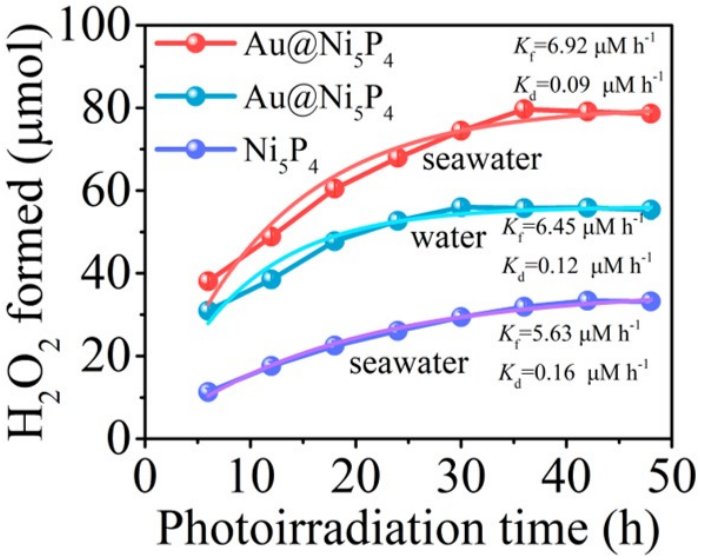

Fig. S4 Time course of H_2O_2 photoproduction and the corresponding fitting curves of $Au@Ni_5P_4$ and Ni_5P_4 in real seawater or water, respectively.

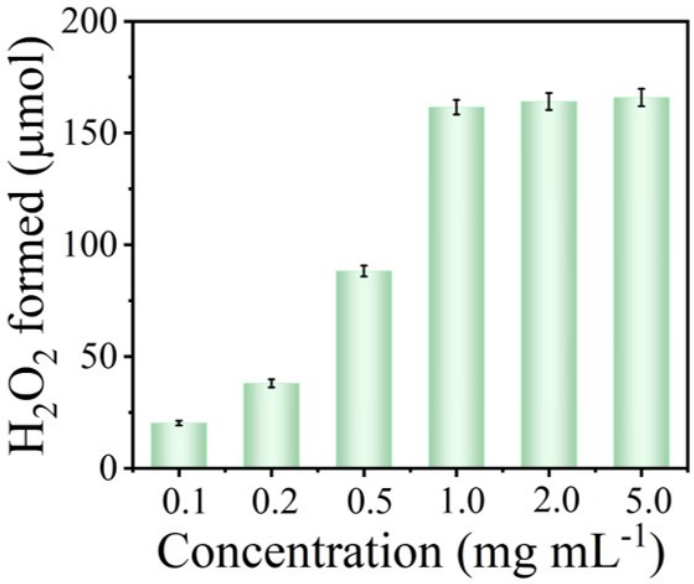

Fig. S5 The photocataltic production of H_2O_2 as a function of mass concentration of $Au@Ni_5P_4$.

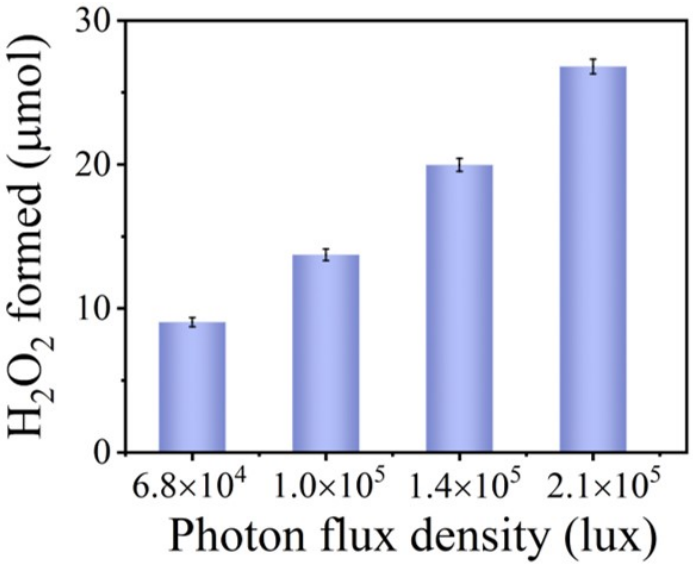

Fig. S6 Photocatalytic H_2O_2 production on Au@Ni_5P_4 under different light intensity for 6 h.

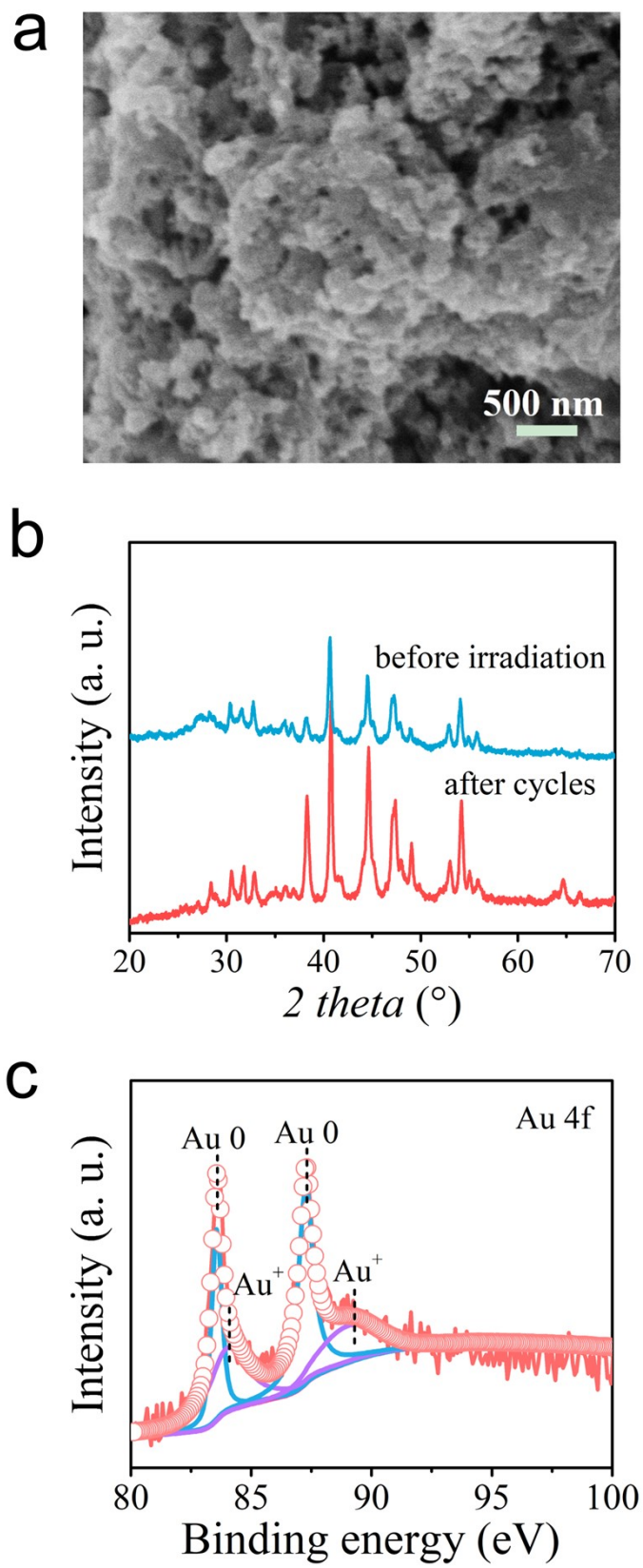

Fig. S7 Stability characterizations of Au@Ni_5P_4 after fifteen cycles of photocatalytic reaction. (a) SEM image. (b) XRD pattern, and (c) High-resolution XPS spectra of Au 4f.

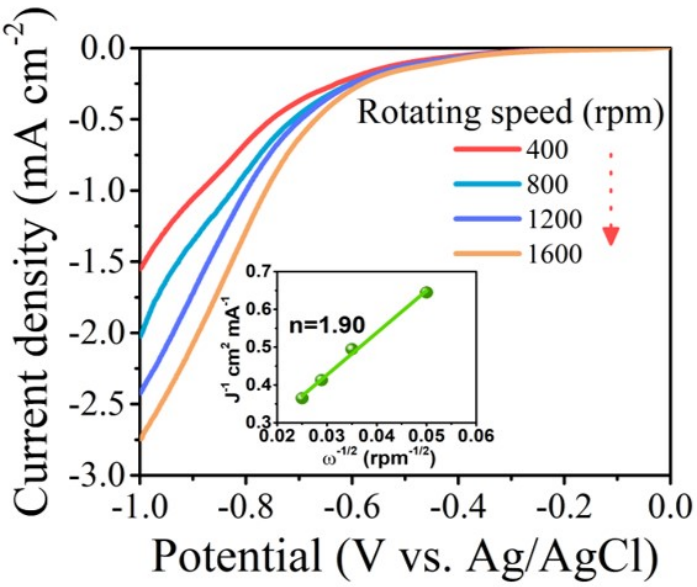

Fig. S8 LSV curves of Ni_5P_4 measured on RDE at different rotating speeds. Inset: the corresponding Koutecky-Levich plot.

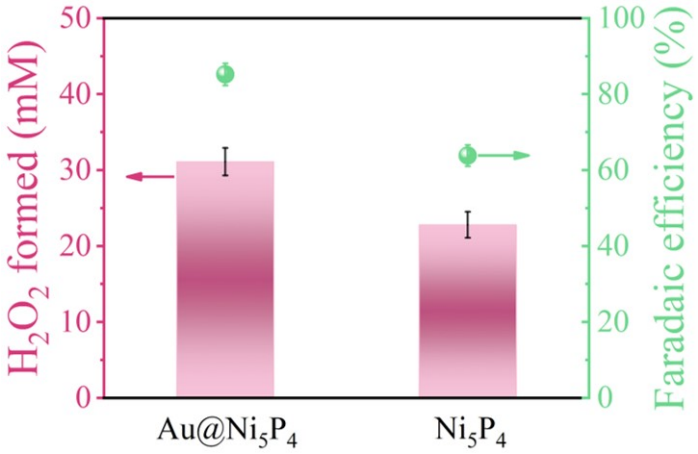

Fig. S9 Concentrations of H_2O_2 formed and the Faradaic efficiency of Au@Ni_5P_4 and Ni_5P_4 cathodes at 50 mA cm^{-2}.

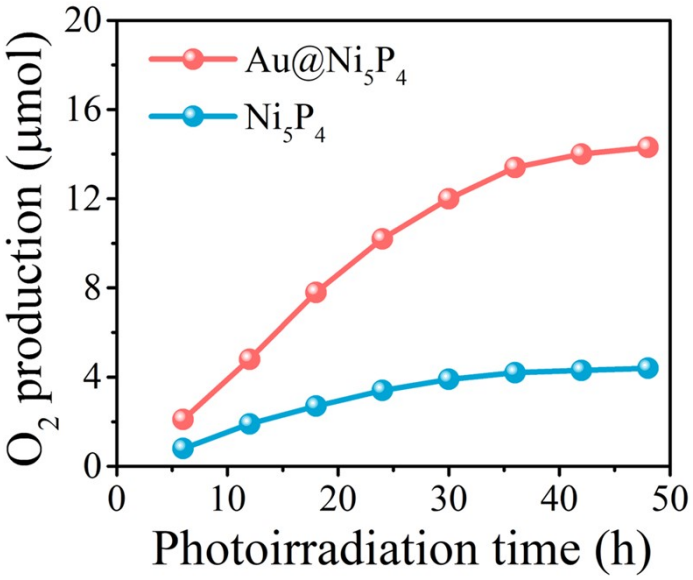

Fig. S10 Amounts of O_2 formed during the half photoreaction.

Table S1 EXAFS fitting parameters at the Au L_3-edge for various samples

Sample	Shell	*CN*[a]	*R*(Å)[b]	σ^2(Å^2)[c]	ΔE_0(eV)[d]	*R* factor
Au foil	Au-Au	12*	2.86±0.03	0.0075±0.0004	4.6±0.4	0.0065
$AuCl_3$	Au-Cl	4.1±0.7	2.31±0.02	0.0038±0.0031	-6.2±1.6	0.0078
Au@Ni_5P_4	Au-P	1.1±0.5	2.34±0.01	0.0090±0.0046	9.5±2.4	0.0179
	Au-Au	7.8±1.9	2.85±0.04	0.0077±0.0018	4.1±1.2	

[a]*CN*, coordination number; [b]*R*, distance between absorber and backscatter atoms; [c]σ^2, Debye-Waller factor to account for both thermal and structural disorders; [d]ΔE_0, inner potential correction; *R* factor indicates the goodness of the fit. S_0^2 was fixed to 0.78, according to the experimental EXAFS fit of Au foil by fixing CN as the known crystallographic value. A reasonable range of EXAFS fitting parameters: $0.700 < S_0^2 < 1.000$; $CN > 0$; $\sigma^2 > 0$ Å^2; $|\Delta E_0| < 10$ eV; *R* factor < 0.02.

Table S2 TRPL data of $Au@Ni_5P_4$ and Ni_5P_4.

Samples	τ_1/ns (A_1)	τ_2/ns (A_2)	τ_A/ns
$Au@Ni_5P_4$	0.88 (64.8%)	6.54 (35.2%)	5.42
Ni_5P_4	0.76 (67.3%)	4.53 (32.7%)	3.56

References

1 Y. Liu, Y. Zhao, Y. Sun, J. Cao, H. Wang, X. Wang, H. Huang, M. Shao, Y. Liu and Z. Kang, A $4e^{-}$-$2e^{-}$ cascaded pathway for highly efficient production of H_2 and H_2O_2 from water photo-splitting at normal pressure, *Appl. Catal. B: Environ.*, 2020, **270**, 118875.

2 Y. Liu, Y. Zhao, Q. Wu, X. Wang, H. Nie, Y. Zhou, H. Huang, M. Shao, Y. Liu and Z. Kang, Charge storage of carbon dot enhances photo-production of H_2 and H_2O_2 over Ni_2P/carbon dot catalyst under normal pressure, *Chem. Eng. J.*, 2021, **409**, 128184.